

Texture Control in a Pseudospin Bose-Einstein Condensate

Gary Ruben, Michael J. Morgan, and David M. Paganin

School of Physics, Monash University, Victoria 3800, Australia

(Received 21 May 2010; revised manuscript received 1 September 2010; published 24 November 2010)

We describe a wave function engineering approach to the formation of textures in nonrotated multicomponent Bose-Einstein condensates. With numerical simulations of a viable two-component condensate experiment, we demonstrate the formation of a ballistically expanding regular lattice texture, composed of half-quantum vortices and spin-2 textures. The formation is described by a linear interference process in which the geometry and phase of three initially separated wave packets provide deterministic control over the resulting lattice texture.

DOI: 10.1103/PhysRevLett.105.220402

PACS numbers: 03.75.Mn, 03.75.Dg, 03.75.Lm

Topological spin textures arise in magnetic materials [1], in director fields of liquid crystals [2], in field theoretic models of particles [3], and in models of the early Universe [4]. Multicomponent Bose-Einstein condensates (BECs) may act as analogues of these and other condensed matter systems, enabling the study of phenomena that may be otherwise inaccessible to experimental investigation.

Bulk rotation of scalar (single-component) BECs provides one method for creating a regular lattice of quantized vortices. The additional spin freedom in rotating multicomponent BECs suggests the existence of related spin lattice textures, which are indeed observed [5]. Experimental production of isolated textures has been demonstrated within pseudospin- $\frac{1}{2}$, spin-1, and spin-2 BECs [6–8].

In this Letter we describe a complementary method for the controlled production of a lattice texture in a multicomponent BEC, which forgoes bulk rotation of the condensate by instead exploiting interference to produce expanding lattices of singly quantized vortices in any or all components. An advantage of this method is that the textures comprising the motif may be directly determined by the vortex-lattice alignment, which depends on the controllable wave packet phases. Isolated textures could be optically retrapped once created by this process.

Nonrotated single-component BECs accommodate regular vortex lattices, created by a three-wave linear interference process [9]. In this scenario, three initially separated BEC wave packets expand and interfere, in an analogous process to a Young’s three-pinhole interferometer [10]. When the initial wave packets are arranged at the corners of an equilateral triangle, the resulting lattice has honeycomb symmetry and can be thought of as a dynamically expanding hexagonal lattice containing unit-charge vortices of one circulation, interleaved with a second similar lattice of vortices with opposite circulation. It is probable that such honeycomb vortex-antivortex (VA) lattices have been experimentally generated in BECs, although this has neither been recognized nor verified directly—see [11,12]. The initial wave packet phases establish particular xy translations of the resulting 2D VA

lattices [9]. By engineering the initial wave packets in a two-component BEC, we exploit this phase dependence to produce VA lattices within each component of a two-component BEC, aligning them to form the dynamically expanding lattice texture. In the example in Fig. 1, the position-dependent state is represented by local Bloch vectors, which project the state onto the surface of a unit Bloch sphere (Fig. 1 inset).

Although a rotating BEC is extended in three spatial dimensions, its resident vortex lattice is primarily 2D in nature, which restricts the topology of any associated texture. The VA lattice is similarly 2D in nature, because the three initial wave packet locations together define a plane. In both cases, axial absorption imaging captures the 2D structure by projecting the density parallel to the vortex core axes. The simplest texture arises when a vortex in one component coincides with a vortex-free region in the second component to create a half-quantum vortex (HQV) [13], which is a counterpart to the Alice string in particle physics [14]; its detection in $^3\text{He}-A$ is sought as evidence of a spin triplet superconducting state in Sr_2RuO_4 [15]. Another example, of relevance here, corresponds to a vortex in one component aligned with a vortex of opposite circulation in the second component. This texture may be thought of as a lower dimensional counterpart to the “spin

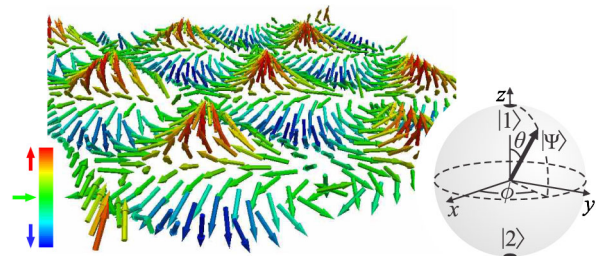


FIG. 1 (color online). A planar lattice texture is created by the interference of a pseudospin- $\frac{1}{2}$ BEC initially separated into three pieces. The hexagonal lattice, visualized with Bloch vectors in this numerical simulation, has a motif containing three textures: one half-quantum vortex of each sign and a spin-2 texture.

vortex” that arises spontaneously in quenched ^{87}Rb spinor condensates [16]. Additional textures in 2D geometries include baby skyrmions [17], merons [18], and planar spin textures [19], whose study has led to insights in reduced-dimensional superfluid or ferromagnetic systems, such as in the case of the quantum Hall effect [20]. We describe a mechanism of lattice-texture formation that extends to three or more arbitrarily located spatially separated spinor BEC pieces with arbitrary initial coherent phases. The mechanism operates in limits where linear interference applies, i.e., when the kinetic energy term dominates the self-interaction term in the Hamiltonian. In this case, the long-range effect of initial coherent wave packet phases establishes the required local phase relationship for vortex production at points in a lattice. This may be contrasted with the Kibble-Zurek (KZ) mechanism [21], in which vortices are created by phase windings generated in neighboring domains by quenching through a phase transition.

In the following, we present simulations of a proposed experiment to generate the lattice texture via the interference of a nonrotating pseudospin- $\frac{1}{2}$ BEC, initially divided into three pieces. Although it is possible to fully control the piece phases and resulting textures, we present a simplified experiment in which the phases are fixed. A planar hexagonal lattice-texture results, with a motif composed of three textures: one HQV of each sign and a spin-2 texture. We classify these textures by their topologies, and present a lattice model whose time-dependent growth is related to the initial BEC geometry.

We numerically model a two-level ^{87}Rb BEC system with $|F=1, m_F=-1\rangle \equiv |1\rangle$ and $|F=2, m_F=+1\rangle \equiv |2\rangle$ using a mean-field approach. These hyperfine states and their coupling behavior have been well studied [22,23] and are convenient for the study of pseudospin- $\frac{1}{2}$ condensates. We performed 2D simulations, corresponding to pancake condensates. This geometry has the advantage that axial ballistic expansion is rapid, due to the initial tight axial confinement. Nonlinear effects, which might otherwise lead to distortion of any lattice and curvature or reconnection of vortex lines, are consequently short-lived. The order parameter field of a single-species BEC whose atoms occupy two internal hyperfine levels is a position-dependent two-component pseudospinor $\Psi(\mathbf{r}) = (\Psi_1(\mathbf{r}), \Psi_2(\mathbf{r}))$, where \mathbf{r} is a position vector [24]. The dynamical evolution of the BEC is governed by two coupled Gross-Pitaevskii Equations (GPEs):

$$i\hbar \frac{\partial \Psi_i}{\partial t} = \left(-\frac{\hbar^2}{2m} \nabla_{\perp}^2 + V_i + \Gamma(t) \sum_{j=1,2} U_{ij} |\Psi_j|^2 \right) \Psi_i, \quad i=1,2, \quad (1)$$

where Ψ_i is the 2D order parameter of component $|i\rangle$ and ∇_{\perp}^2 is a 2D Laplacian. The self-interaction parameter $U_{ij} = 4\pi\hbar^2 a_{ij}/m$ depends on the intra- and intercomponent s -wave scattering lengths a_{ij} and the mass m of an atom of the condensed species; there are three independent

scattering lengths, since $a_{12} = a_{21}$. A time-dependent factor $\Gamma(t)$ results from the reduction from 3D to 2D, as described below. The normalization condition is $\sum_i \int |\Psi_i|^2 d\mathbf{r} = N$, where the total number of atoms N is preserved independently of the internal spin state.

We use the state-dependent scattering lengths of Mertes *et al.* [23]: $a_{11} = 100.40a_0$, $a_{22} = 95.00a_0$, and $a_{21} \equiv a_{12} = 97.66a_0$, where a_0 is the Bohr radius. The condensate contains $N = 50\,000$ atoms of ^{87}Rb , each of mass $m = 1.4188 \times 10^{-25}\text{kg}$. This relatively small population was chosen to minimize nonlinear perturbative effects and maximize lattice regularity.

Initially the BEC is tightly trapped in the axial direction, producing a pancake geometry, and further divided into three pieces by trapping within three transverse Gaussian potential wells, such as would be formed by three red-detuned lasers. The initial equilibrium condensate profile is established with all atoms in $|1\rangle$ by numerically evolving Eq. (1) through imaginary time. In simulations, the numerical procedure establishes a uniform phase ($\varphi_1 = \varphi_2 = \varphi_3$) for the wave packets, which fixes the translation of the resulting lattice texture. However, in typical experiments the initial wave packet phases are random, resulting in the lattice being randomly translated. Therefore, in an experiment, both components must be imaged simultaneously to correctly reconstruct the lattice-texture structure. This might be performed by dual state imaging [25] or by minimally destructive phase contrast imaging [26].

Having established the initial profile, we immediately remove all trap potentials V_i at $t=0$. We account for ballistic expansion along the axial direction by assuming each piece to be a noninteracting gas with a Gaussian axial profile. Upon trap removal, the resulting rapid axial expansion and associated decrease in nonlinear coupling are modeled by $\Gamma(t) = [m\omega/(2\pi\hbar)]^{1/2} (1+t^2\omega^2)^{-1/2}$, where ω is the angular frequency of the axial harmonic trap initially confining the condensate. We use $\omega = 500\text{ rad s}^{-1}$, corresponding to a pancake geometry.

We simulate the application of a two-photon $\pi/2$ pulse to excite half the atoms to $|2\rangle$ (Fig. 2). This models an optical process involving two lasers, coupling $|1\rangle$ and $|2\rangle$ via an intermediate level. The $\pi/2$ pulse may be applied either immediately before or after trap removal. The overall translation of each VA lattice depends only on the

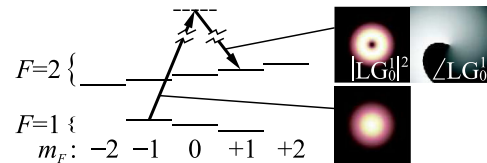


FIG. 2 (color online). ^{87}Rb hyperfine levels $|F=1, m_F=-1\rangle \equiv |1\rangle$ and $|F=2, m_F=+1\rangle \equiv |2\rangle$ are optically coupled with Gaussian and Laguerre-Gauss (LG) lasers, whose intensity profiles are shown. The $\text{LG}_{p=0}^{\ell=1}$ phase is also shown winding from $-\pi$ (black) to $+\pi$ (white).

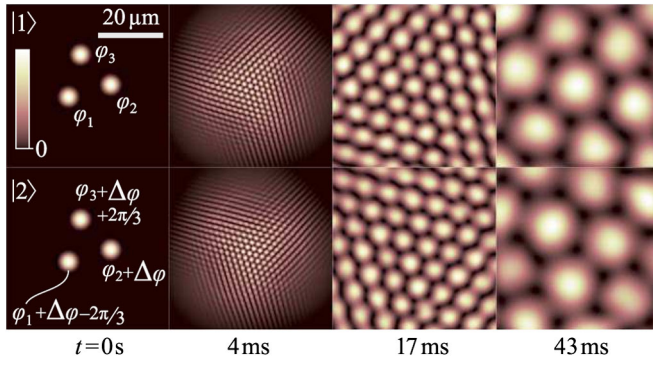


FIG. 3 (color online). Numerical simulations of a two-component three-piece BEC generate vortex-antivortex lattices as the wave packets expand and interfere. For the initial phases shown, the lattices align as is evident in Fig. 4(a).

relative phases of the initial wave packets [9]. Although intracomponent phases are uncontrolled in typical experiments, full control over the intercomponent phase may be realized by spatially localized Raman beam pairs focused on each wave packet. Atoms excited to $|2\rangle$ thereby acquire relative phases that produce a lattice which is predictably aligned with the lattice in $|1\rangle$, enabling production of a continuum of related lattice textures. In our simplified example, we instead employ a Laguerre-Gauss $\text{LG}_{p=0}^{\ell=1}$ mode in one of the coupling beams to establish wave packet phases $\varphi_1 + \Delta\varphi - 2\pi/3$, $\varphi_2 + \Delta\varphi$, and $\varphi_3 + \Delta\varphi + 2\pi/3$ for atoms in $|2\rangle$ [27]. The phase offset $\Delta\varphi$ has no effect on lattice translation [9]. The LG beam wave front confers phase gradients on each wave packet in $|2\rangle$. Any effects of this nonuniformity are minimized due to the initial tight transverse confinement.

The BEC then evolves governed by Eq. (1), resulting in the axially projected probability densities $|\Psi_i|^2$ shown in Fig. 3. A honeycomb VA lattice is formed in each component, resulting from interference of the expanding wave packets. The equal initial phases ($\varphi_1 = \varphi_2 = \varphi_3$) produce the particular lattice translations shown. The final frame of this figure shows individual components $|\Psi_i|^2$ at $t = 43$ ms, corresponding to the lattice texture in Fig. 1.

We now consider the three textures that combine in the motif of Fig. 1, corresponding to alignments of vortices in Fig. 4(a). We examine these textures in more detail in Fig. 5, using simulations at $t = 69$ ms. Vortex and antivortex locations in each component are identified in Fig. 5(a). Because textures extend over a local neighborhood of the field, we specify three circular bounded regions, labeled (i), (ii), and (iii), centered on the vortex cores. Each boundary lies approximately halfway to the nearest neighboring vortex core. The same boundaries are shown in Fig. 5(b), which plots the field of Bloch vectors with lengths scaled by local density, and identifies the three texture types. In crystallographic terms, the three textures constitute a motif, within a hexagonal lattice.

Region (i) in Fig. 5 corresponds to a spin-2 texture with zero net mass current, associated with two constituent

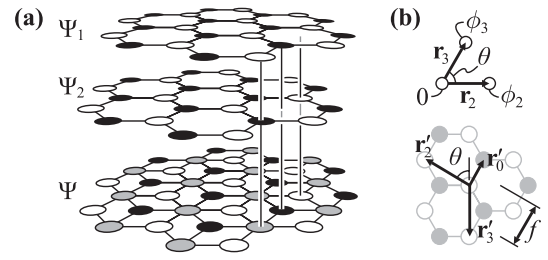


FIG. 4. (a) Lattices containing vortices (white circles) and antivortices (black circles) form in components Ψ_1 and Ψ_2 . Three combinations form different textures in $\Psi \equiv (\Psi_1, \Psi_2)$. Gray circles indicate an aligned vortex and antivortex in the two components. (b) Wave packets with centers given by $\mathbf{r}_1 \equiv \mathbf{0}$, \mathbf{r}_2 , \mathbf{r}_3 have relative phases 0 , ϕ_2 , ϕ_3 , respectively. The resulting vortex-antivortex lattice basis vectors are \mathbf{r}'_2 and \mathbf{r}'_3 , with a motif containing a vortex and antivortex separated by \mathbf{r}'_0 . Fringe spacing f is a convenient measure of unit cell size.

unit-charge vortices of opposite sign that reside in different components. In traversing a small closed contour about the vortex core in Fig. 5(b) once, vector projections wrap the Bloch sphere twice near the equator, with winding number 2. As contours of larger radius are traversed, the projections deviate from the equator toward the Bloch sphere poles. This texture is similar to spin textures described elsewhere in a 2D spin system [19] and in three-component spin textures [16].

Regions (ii) and (iii) in Fig. 5 are centered on a vortex in one or other of the components. These correspond to HQVs. The Bloch vectors within these regions cover the Bloch sphere hemisphere corresponding to the sign of the HQV. As the lattice expands, projections of vectors on the boundary approach the Bloch sphere equator. An HQV has wrapping number 1 for a hemispherical order parameter space, associated with its constituent unit-charge vortex. It covers a 2π solid angle and is thus a 2π defect whose sign depends on both the vortex sign and its resident component. Similarly, boundary projections of the spin-2 texture asymptotically approach Bloch-sphere lines of longitude. If these boundaries are “healed,” the sphere has wrapping number 2 and the texture is identifiable as an 8π defect.

Having discussed the topology of the isolated textures, we now describe the lattice texture. The isolated textures

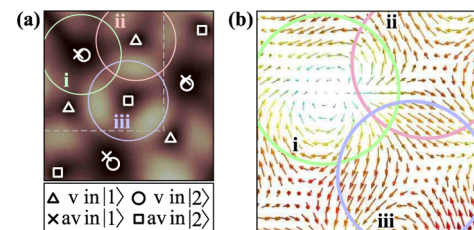


FIG. 5 (color online). Three texture types within the motif: (i) a spin-2 defect, (ii) a (+) HQV, and (iii) a (-) HQV. (a) Vortex (v) and antivortex (av) cores are overlaid on a map of $|\Psi_1 \Psi_2|$. (b) Bloch vectors are shown normalized to $(\Psi_1^2 + \Psi_2^2)^{1/2}$.

expand along with the evolving lattice according to previously described expressions for vortex core locations in a model of interfering Gaussian wave packets [9]. For vortices to be produced by interference, the contributions from each expanding packet must be approximately equal. This establishes a spatiotemporal condition, which limits lattice extent and describes its growth by vortex formation at the boundary of an expanding circular envelope [9]. This envelope expands within a second expanding envelope that defines the extent of the BEC cloud, associated with a threshold density of the condensate tail. Two-source interference fringes are visible in the annular region between these envelopes (Fig. 3 at 4 ms).

By evaluating the locations of two adjacent vortices of the same sign within the inner envelope, we find that the lattice basis vectors [Fig. 4(b)] have lengths

$$|\mathbf{r}'_2| = \pi/(r_3\alpha \sin\theta), \quad |\mathbf{r}'_3| = \pi/(r_2\alpha \sin\theta), \quad (2)$$

where $r_j \equiv |\mathbf{r}_j|$ are the source spacings, and θ is the interior angle at the origin of the triangle of wave packets [Fig. 4(b)]. These expressions depend linearly on a time-dependent lattice scaling factor $\alpha = m\hbar t/[2(\hbar t)^2 + 2m^2(\hbar/\Delta p)^4]$, which assumes that the packets share a single initial momentum uncertainty Δp ; i.e., are all of equal initial size. Because the lattice growth in this linear model is independent of condensate density, vortex lines remain straight and parallel despite any density anisotropy arising from ballistic expansion along their length. The distance f in Fig. 4(b) corresponds to the bright fringe spacing, measured experimentally by Henderson *et al.* [12]. For $r \equiv r_2 = r_3$ and $\theta = \pi/3$, $f = |\mathbf{r}'_3|\sqrt{3}/2 = \pi/(r\alpha)$. The spacing of adjacent vortices and antivortices in the VA lattice is

$$|\mathbf{r}'_0| = \pi(r_2^2 + 2r_2r_3 \cos\theta + r_3^2)^{1/2}/(3r_2r_3\alpha \sin\theta). \quad (3)$$

If $r \equiv r_2 = r_3$ and $\theta = \pi/3$, then $|\mathbf{r}'_0| = 2\pi/(3r\alpha)$.

We have shown with numerical simulations that a lattice texture forms in a nonrotated two-component BEC, initially separated into three pieces, and subsequently allowed to expand and interfere. We created an expanding hexagonal lattice texture by employing spatiotemporal wave function engineering to determine specific relative phases of the initial pieces and arrange them at the corners of an equilateral triangle. By employing a Laguerre-Gauss beam in the phase-engineering task, the lattice was created with a motif composed of two half-quantum vortices of opposite signs and one spin-2 texture, both being relevant examples in related condensed matter systems. More generally, the method extends to deterministic production of related lattice textures. Whereas initially positioning the pieces to form an equilateral triangle generates a honeycomb lattice, different (triangular) arrangements may generate other geometries, including rectangular lattices from right triangles. The textures in the motif decorating this lattice are composed of singly quantized vortices arranged deterministically within a bounded region of comparable

size to the lattice parameter, in any or all components of a multicomponent BEC. The method may be applied to produce higher order textures by considering additional components not spin coupled to the existing states. Related textures will be produced in spinor condensates, in which the states within a single manifold are populated and spin-spin interactions are considered.

G.R. thanks T.P. Simula, K. Helmerson, L.D. Turner, R.P. Anderson, and E.J. Mueller for helpful discussions, and acknowledges Australian government support.

-
- [1] S. Mühlbauer *et al.*, *Science* **323**, 915 (2009).
 - [2] C. Noël, *Acta Polym.* **48**, 335 (1997).
 - [3] T.H.R. Skyrme, *Proc. R. Soc. A* **260**, 127 (1961).
 - [4] A. Vilenkin, *Phys. Rev. D* **23**, 852 (1981).
 - [5] T. Mizushima, N. Kobayashi, and K. Machida, *Phys. Rev. A* **70**, 043613 (2004); J.W. Reijnders *et al.*, *ibid.* **69**, 023612 (2004); E.J. Mueller, *ibid.* **69**, 033606 (2004); V. Schweikhard *et al.*, *Phys. Rev. Lett.* **93**, 210403 (2004).
 - [6] M.R. Matthews *et al.*, *Phys. Rev. Lett.* **83**, 2498 (1999).
 - [7] A.E. Leanhardt *et al.*, *Phys. Rev. Lett.* **90**, 140403 (2003).
 - [8] L.S. Leslie *et al.*, *Phys. Rev. Lett.* **103**, 250401 (2009).
 - [9] G. Ruben, D.M. Paganin, and M.J. Morgan, *Phys. Rev. A* **78**, 013631 (2008).
 - [10] G. Ruben and D.M. Paganin, *Phys. Rev. E* **75**, 066613 (2007); **76**, 029901(E) (2007).
 - [11] D.R. Scherer *et al.*, *Phys. Rev. Lett.* **98**, 110402 (2007); R. Carretero-González *et al.*, *Phys. Rev. A* **77**, 033625 (2008).
 - [12] K. Henderson *et al.*, *New J. Phys.* **11**, 043030 (2009).
 - [13] M.C. Cross and W.F. Brinkman, *J. Low Temp. Phys.* **27**, 683 (1977).
 - [14] U. Leonhardt and G.E. Volovik, *JETP Lett.* **72**, 46 (2000); T. Isoshima, K. Machida, and T. Ohmi, *J. Phys. Soc. Jpn.* **70**, 1604 (2001).
 - [15] V. Vakaryuk and A.J. Leggett, *Phys. Rev. Lett.* **103**, 057003 (2009).
 - [16] L.E. Sadler *et al.*, *Nature (London)* **443**, 312 (2006); H. Saito, Y. Kawaguchi, and M. Ueda, *Phys. Rev. Lett.* **96**, 065302 (2006).
 - [17] B.M.A.G. Piette, B.J. Schoers, and W.J. Zakrzewski, *Z. Phys. C* **65**, 165 (1995).
 - [18] C.G. Allan, R. Dashen, and D.J. Gross, *Phys. Lett. B* **66**, 375 (1977). (Note that in this reference the name of the first author is misspelled. The first author is Curtis G. Callan, Jr.)
 - [19] N.D. Mermin, *Rev. Mod. Phys.* **51**, 591 (1979).
 - [20] T. Ando, Y. Matsumoto, and Y. Uemura, *J. Phys. Soc. Jpn.* **39**, 279 (1975).
 - [21] T.W.B. Kibble, *J. Phys. A* **9**, 1387 (1976).
 - [22] M.R. Matthews *et al.*, *Phys. Rev. Lett.* **81**, 243 (1998).
 - [23] K.M. Mertes *et al.*, *Phys. Rev. Lett.* **99**, 190402 (2007).
 - [24] T.-L. Ho, *Phys. Rev. Lett.* **81**, 742 (1998); T. Ohmi and K. Machida, *J. Phys. Soc. Jpn.* **67**, 1822 (1998).
 - [25] R.P. Anderson *et al.*, *Phys. Rev. A* **80**, 023603 (2009).
 - [26] L.D. Turner, K.F.E.M. Domen, and R.E. Scholten, *Phys. Rev. A* **72**, 031403(R) (2005).
 - [27] M.F. Andersen *et al.*, *Phys. Rev. Lett.* **97**, 170406 (2006).